INTERNATIONAL JOURNAL FOR NUMERICAL METHODS IN ENGINEERING
Int. J. Numer. Meth. Engng 2002; **55**:613–628 (DOI: 10.1002/nme.518)

A new finite-element formulation for electromechanical boundary value problems

Chad M. Landis*,†

Department of Mechanical Engineering and Materials Science, MS 321, Rice University, P.O. Box 1892, Houston, TX 77251, U.S.A.

SUMMARY

In this paper, a new finite-element formulation for the solution of electromechanical boundary value problems is presented. As opposed to the standard formulation that uses scalar electric potential as nodal variables, this new formulation implements a vector potential from which components of electric displacement are derived. For linear piezoelectric materials with positive definite material moduli, the resulting finite-element stiffness matrix from the vector potential formulation is also positive definite. If the material is non-linear in a fashion characteristic of ferroelectric materials, it is demonstrated that a straightforward iterative solution procedure is unstable for the standard scalar potential formulation, but stable for the new vector potential formulation. Finally, the method is used to compute fields around a crack tip in an idealized non-linear ferroelectric material, and results are compared to an analytical solution. Copyright © 2002 John Wiley & Sons, Ltd.

KEY WORDS: finite-element method; vector potential; piezoelectricity; ferroelectricity

1. INTRODUCTION

Since the original work of Allik and Hughes [1] in 1970, a rather large literature has developed on finite-element methods for linear piezoelectric materials and structures [2]. However, much less attention has focused on problems involving non-linear electromechanical constitutive response, with the exception of the work of Ghandi and Hagood [3]. It will be demonstrated in Section 5 of this paper, that difficulties arise in the solution of electrically non-linear problems when the standard, scalar potential, finite-element formulation developed in Reference [1] is used. In order to overcome these difficulties, Ghandi and Hagood [3] developed a hybrid finite-element formulation that employs the standard displacement and electric potential nodal degrees of freedom along with additional electric displacement degrees of freedom within the element. In this work, an alternative approach that implements a vector potential formulation is developed.

*Correspondence to: Chad M. Landis, Department of Mechanical Engineering and Materials Science, MS 321, Rice University, P.O. Box 1892, Houston, TX 77251, U.S.A.
†E-mail: landis@rice.edu

Received 6 June 2001
Revised 5 November 2001
Accepted 30 December 2001

As opposed to the standard scalar potential formulation, where the electric potential is interpolated from nodal quantities and the electric field derived from the electric potential; the vector potential formulation derives the *electric displacement* from the components of the vector potential which are the interpolated nodal quantities. Advantages of the vector potential formulation include a positive definite stiffness matrix and numerical stability for non-linear electrical material behaviour characteristic of ferroelectric ceramics. The disadvantages of the method include an increase in the number of nodal degrees of freedom for three-dimensional problems and the inability of the method to account for a free charge density within the material volume.

The body of the paper is concerned with comparing the scalar and vector potential formulations. Section 2 is devoted to introducing the equations governing a dynamic electromechanical boundary value problem. Section 3 develops the scalar and vector potential formulations, and then compares features of the stiffness matrices and system sizes. Section 4 compares the scalar and vector potential formulations numerically by using each to solve a linear piezoelectric problem and investigating the convergence with respect to mesh size. Section 5 presents a simple numerical stability analysis of the two formulations for a one-dimensional electrical system with non-linear material behaviour. Section 6 implements the vector potential formulation to solve for the electrical fields around a crack tip in an idealized ferroelectric material, and compares the numerical results to a known analytical solution. Finally, Section 7 summarizes the merits of the new vector potential formulation for the solution of non-linear electromechanical boundary value problems.

2. GOVERNING EQUATIONS

In this section, the equations governing a small deformation, small electric field, mechanically dynamic but electrically quasi-static, isothermal electromechanical boundary value problem will be reviewed. Throughout this section, standard index notation is utilized with summation implied over repeated indices and the subscript $_{,j}$ representing differentiation with respect to the x_j co-ordinate direction.

Consider a volume of material, V, bounded by the surface, S. Newton's second law is given by

$$\sigma_{ji,j} + b_i = \rho \ddot{u}_i \quad \text{in } V \tag{1}$$

and

$$\sigma_{ji} n_j = t_i \quad \text{on } S \tag{2}$$

where σ_{ij} is the symmetric Cauchy stress tensor, b_i is the body force per unit volume, ρ is the mass density of the material, u_i are the components of the material displacement, n_i is a unit vector normal to the surface directed outward from the volume, and t_i is the traction applied to the surface. The superposed double dot represents a second derivative with respect to time.

The infinitesimal strain-displacement compatibility conditions are

$$\varepsilon_{ij} = \tfrac{1}{2}(u_{i,j} + u_{j,i}) \tag{3}$$

where ε_{ij} is the infinitesimal strain tensor.

Gauss' law is written as

$$D_{i,i} = q^v \quad \text{in } V \tag{4}$$

and

$$D_i n_i = -q^s \quad \text{on } S \tag{5}$$

where D_i is the electric displacement, q^v is the free charge per unit volume in V and q^s is the free charge per unit area (also accounting for the effective charge due to material outside of V) residing on S.

Under quasi-static conditions the electric field, E_i, can be written as the gradient of a potential, ϕ, such that

$$E_i = -\phi_{,i} \tag{6}$$

Finally, the four forms of the linear piezoelectric constitutive law about a fixed remanent strain and polarization state are given by

$$\varepsilon_{ij} - \varepsilon_{ij}^{\mathrm{r}} = s_{ijkl}^{E}\sigma_{kl} + d_{kij}E_k, \quad D_i - P_i^{\mathrm{r}} = d_{ikl}\sigma_{kl} + \kappa_{ij}^{\sigma}E_j \tag{7}$$

$$\sigma_{ij} = c_{ijkl}^{E}(\varepsilon_{kl} - \varepsilon_{kl}^{\mathrm{r}}) - e_{kij}E_k, \quad D_i - P_i^{\mathrm{r}} = e_{ikl}(\varepsilon_{kl} - \varepsilon_{kl}^{\mathrm{r}}) + \kappa_{ij}^{\varepsilon}E_j \tag{8}$$

$$\sigma_{ij} = c_{ijkl}^{D}(\varepsilon_{kl} - \varepsilon_{kl}^{\mathrm{r}}) - h_{kij}(D_k - P_k^{\mathrm{r}}), \quad E_i = -h_{ikl}(\varepsilon_{kl} - \varepsilon_{kl}^{\mathrm{r}}) + \beta_{ij}^{\varepsilon}(D_j - P_j^{\mathrm{r}}) \tag{9}$$

$$\varepsilon_{ij} - \varepsilon_{ij}^{\mathrm{r}} = s_{ijkl}^{D}\sigma_{kl} + g_{kij}(D_k - P_k^{\mathrm{r}}), \quad E_i = -g_{ikl}\sigma_{kl} + \beta_{ij}^{\sigma}(D_j - P_j^{\mathrm{r}}) \tag{10}$$

where $\varepsilon_{ij}^{\mathrm{r}}$ and P_i^{r} are the remanent strain and polarization, s_{ijkl}^{E}, s_{ijkl}^{D}, c_{ijkl}^{E} and c_{ijkl}^{D} are fourth rank tensors of elasticity, d_{kij}, e_{kij}, h_{kij} and g_{kij} are third rank tensors of piezoelectricity and κ_{ij}^{σ}, $\kappa_{ij}^{\varepsilon}$, β_{ij}^{σ} and β_{ij}^{ε} are second rank dielectric tensors. Note that any set of moduli can be manipulated algebraically to yield any other set. The constitutive form of Equation (7) is commonly used to report experimentally measured moduli, that of Equation (8) is required for the standard scalar potential finite-element formulation, and the form in Equation (9) will be used in the vector potential finite-element formulation.

Finally, Equations (1)–(6) can be written in the following two weak forms as:

$$\int_V \rho\ddot{u}_i\delta u_i \,\mathrm{d}V + \int_V \sigma_{ij}\delta\varepsilon_{ij} - D_i\delta E_i \,\mathrm{d}V = \int_V b_i\delta u_i - q^v\delta\phi \,\mathrm{d}V + \int_S t_i\delta u_i - q^s\delta\phi \,\mathrm{d}S \tag{11}$$

or

$$\int_V \rho\ddot{u}_i\delta u_i \,\mathrm{d}V + \int_V \sigma_{ij}\delta\varepsilon_{ij} + E_i\delta D_i \,\mathrm{d}V = \int_V b_i\delta u_i + \phi\delta q^v \,\mathrm{d}V + \int_S t_i\delta u_i + \phi\delta q^s \,\mathrm{d}S \tag{12}$$

3. FINITE-ELEMENT FORMULATIONS

In the following formulations vector–matrix notation will be used where the field quantities are given as

$$\begin{aligned} \{\mathbf{u}\} &= \{\, u_x \;\; u_y \;\; u_z \,\}^{\mathrm{T}}, \quad \{\mathbf{E}\} = \{\, E_x \;\; E_y \;\; E_z \,\}^{\mathrm{T}}, \quad \{\mathbf{D}\} = \{\, D_x \;\; D_y \;\; D_z \,\}^{\mathrm{T}} \\ \{\boldsymbol{\varepsilon}\} &= \{\, \varepsilon_{xx} \;\; \varepsilon_{yy} \;\; \varepsilon_{zz} \;\; 2\varepsilon_{yz} \;\; 2\varepsilon_{xz} \;\; 2\varepsilon_{xy} \,\}^{\mathrm{T}}, \quad \{\boldsymbol{\sigma}\} = \{\, \sigma_{xx} \;\; \sigma_{yy} \;\; \sigma_{zz} \;\; \sigma_{yz} \;\; \sigma_{xz} \;\; \sigma_{xy} \,\}^{\mathrm{T}} \end{aligned} \tag{13}$$

etc., and the nodal quantities will be represented by $\{\mathbf{u}^{\mathbf{n}}\}$ and $\{\boldsymbol{\phi}^{\mathbf{n}}\}$. Equations (8) and (9) are then written in matrix form as

$$\{\boldsymbol{\sigma}\} = [\mathbf{c}^{\mathbf{E}}](\{\boldsymbol{\varepsilon}\} - \{\boldsymbol{\varepsilon}^{\mathbf{r}}\}) - [\mathbf{e}]\{\mathbf{E}\}, \quad \{\mathbf{D}\} = [\mathbf{e}]^{\mathrm{T}}(\{\boldsymbol{\varepsilon}\} - \{\boldsymbol{\varepsilon}^{\mathbf{r}}\}) + [\boldsymbol{\kappa}^{\varepsilon}]\{\mathbf{E}\} + \{\mathbf{P}^{\mathbf{r}}\} \tag{14}$$

and

$$\{\boldsymbol{\sigma}\} = [\mathbf{c}^{\mathbf{D}}](\{\boldsymbol{\varepsilon}\} - \{\boldsymbol{\varepsilon}^{\mathbf{r}}\}) - [\mathbf{h}](\{\mathbf{D}\} - \{\mathbf{P}^{\mathbf{r}}\}), \{\mathbf{E}\} = -[\mathbf{h}]^{\mathrm{T}}(\{\boldsymbol{\varepsilon}\} - \{\boldsymbol{\varepsilon}^{\mathbf{r}}\}) + [\boldsymbol{\beta}^{\varepsilon}](\{\mathbf{D}\} - \{\mathbf{P}^{\mathbf{r}}\}) \tag{15}$$

3.1. The standard scalar potential formulation

As noted by Allik and Hughes [1], the standard formulation exploits the similarities in the mathematical structure governing the distributions of electrical and mechanical fields, Equations (1)–(6). In the standard scalar potential formulation, the displacements and the electric potential are interpolated from the associated nodal quantities as

$$\{\mathbf{u}\} = [\mathbf{N}^{\mathbf{u}}]\{\mathbf{u}^{\mathbf{n}}\} \quad \text{and} \quad \phi = [\mathbf{N}^{\boldsymbol{\phi}}]\{\boldsymbol{\phi}^{\mathbf{n}}\} \tag{16}$$

The strains and electric field components can then be derived from the nodal variables as

$$\{\boldsymbol{\varepsilon}\} = [\mathbf{B}^{\mathbf{u}}]\{\mathbf{u}^{\mathbf{n}}\} \quad \text{and} \quad \{\mathbf{E}\} = -[\mathbf{B}^{\boldsymbol{\phi}}]\{\boldsymbol{\phi}^{\mathbf{n}}\} \tag{17}$$

The matrices $[\mathbf{B}^{\mathbf{u}}]$ and $[\mathbf{B}^{\boldsymbol{\phi}}]$ are given as

$$[\mathbf{B}^{\mathbf{u}}] = \begin{bmatrix} \partial_x & 0 & 0 \\ 0 & \partial_y & 0 \\ 0 & 0 & \partial_z \\ 0 & \partial_z & \partial_y \\ \partial_z & 0 & \partial_x \\ \partial_y & \partial_x & 0 \end{bmatrix} [\mathbf{N}^{\mathbf{u}}] \quad \text{and} \quad [\mathbf{B}^{\boldsymbol{\phi}}] = \begin{Bmatrix} \partial_x \\ \partial_y \\ \partial_z \end{Bmatrix} [\mathbf{N}^{\boldsymbol{\phi}}] \tag{18}$$

where ∂_i represents partial differentiation with respect to the i co-ordinate direction. Equation (11) then yields the finite-element equations

$$\begin{aligned} [\mathbf{m}]\{\ddot{\mathbf{u}}^{\mathbf{n}}\} + [\mathbf{K}^{\mathbf{uu}}]\{\mathbf{u}^{\mathbf{n}}\} + [\mathbf{K}^{\mathbf{u}\boldsymbol{\phi}}]\{\boldsymbol{\phi}^{\mathbf{n}}\} &= \int_V [\mathbf{B}^{\mathbf{u}}]^{\mathrm{T}}\{\boldsymbol{\sigma}^{\mathbf{r}}\}\,\mathrm{d}V + \int_V [\mathbf{N}^{\mathbf{u}}]^{\mathrm{T}}\{\mathbf{b}\}\,\mathrm{d}V + \int_S [\mathbf{N}^{\mathbf{u}}]^{\mathrm{T}}\{\mathbf{t}\}\,\mathrm{d}S \\ [\mathbf{K}^{\boldsymbol{\phi}\mathbf{u}}]\{\mathbf{u}^{\mathbf{n}}\} + [\mathbf{K}^{\boldsymbol{\phi}\boldsymbol{\phi}}]\{\boldsymbol{\phi}^{\mathbf{n}}\} &= -\int_V [\mathbf{B}^{\boldsymbol{\phi}}]^{\mathrm{T}}\{\mathbf{D}^{\mathbf{r}}\}\,\mathrm{d}V - \int_V [\mathbf{N}^{\boldsymbol{\phi}}]^{\mathrm{T}} q^v\,\mathrm{d}V - \int_S [\mathbf{N}^{\boldsymbol{\phi}}]^{\mathrm{T}} q^s\,\mathrm{d}S \end{aligned} \tag{19}$$

where

$$\begin{aligned} [\mathbf{K}^{\mathbf{uu}}] &= \int_V [\mathbf{B}^{\mathbf{u}}]^{\mathrm{T}}[\mathbf{c}^{\mathbf{E}}][\mathbf{B}^{\mathbf{u}}]\,\mathrm{d}V, \quad [\mathbf{K}^{\mathbf{u}\boldsymbol{\phi}}] = \int_V [\mathbf{B}^{\mathbf{u}}]^{\mathrm{T}}[\mathbf{e}][\mathbf{B}^{\boldsymbol{\phi}}]\,\mathrm{d}V \\ [\mathbf{K}^{\boldsymbol{\phi}\mathbf{u}}] &= \int_V [\mathbf{B}^{\boldsymbol{\phi}}]^{\mathrm{T}}[\mathbf{e}]^{\mathrm{T}}[\mathbf{B}^{\mathbf{u}}]\,\mathrm{d}V, \quad [\mathbf{K}^{\boldsymbol{\phi}\boldsymbol{\phi}}] = -\int_V [\mathbf{B}^{\boldsymbol{\phi}}]^{\mathrm{T}}[\boldsymbol{\kappa}^{\varepsilon}][\mathbf{B}^{\boldsymbol{\phi}}]\,\mathrm{d}V \\ [\mathbf{m}] &= \int_V [\mathbf{N}^{\mathbf{u}}]^{\mathrm{T}}\rho[\mathbf{N}^{\mathbf{u}}]\,\mathrm{d}V \end{aligned} \tag{20}$$

and

$$\{\boldsymbol{\sigma}^{\mathbf{r}}\} = [\mathbf{c}^{\mathbf{E}}]\{\boldsymbol{\varepsilon}^{\mathbf{r}}\}$$
$$\{\mathbf{D}^{\mathbf{r}}\} = -[\mathbf{e}]^{\mathrm{T}}\{\boldsymbol{\varepsilon}^{\mathbf{r}}\} + \{\mathbf{P}^{\mathbf{r}}\} \tag{21}$$

Equation (19) represents the standard finite-element formulation for piezoelectric solids. Note that in most calculations the first terms associated with the remanent state on the right-hand sides of Equation (19) are taken to be zero. It is physically reasonable to assume that the remanent strain is equal to zero as long as it does not change. However, a similar treatment of the remanent polarization is not suitable unless the electrical boundary conditions are adjusted appropriately.

3.2. *Vector potential formulation*

As opposed to the scalar potential formulation, the vector potential formulation exploits the similarities in the constitutive (i.e. thermodynamic) structure between the electrical and mechanical variables, Equation (9). The vector potential formulation is restricted to problems where the free charge density in the volume is equal to zero. In other words, Equation (4) is re-written as

$$D_{i,i} = 0 \quad \text{in } V \tag{22}$$

Then Equation (22) can automatically be satisfied by the vector potential, ψ_i, if

$$D_i = \in_{ijk} \psi_{j,k} \tag{23}$$

where $\in_{ijk}$ is the permutation tensor. Now, the nodal degrees of freedom consist of the three displacements and the three components of the vector potential. The vector potential field will be represented by $\{\boldsymbol{\psi}\}$ and the associated nodal quantities by $\{\boldsymbol{\psi}^{\mathbf{n}}\}$. Along with the weak form of Equation (12), the following interpolations are the foundation of the formulation:

$$\{\mathbf{u}\} = [\mathbf{N}^{\mathbf{u}}]\{\mathbf{u}^{\mathbf{n}}\} \quad \text{and} \quad \{\boldsymbol{\psi}\} = [\mathbf{N}^{\boldsymbol{\psi}}]\{\boldsymbol{\psi}^{\mathbf{n}}\} \tag{24}$$

Then the strains and electric displacement components are derived from the displacements and the vector potential as

$$\{\boldsymbol{\varepsilon}\} = [\mathbf{B}^{\mathbf{u}}]\{\mathbf{u}^{\mathbf{n}}\} \quad \text{and} \quad \{\mathbf{D}\} = [\mathbf{B}^{\boldsymbol{\psi}}]\{\boldsymbol{\psi}^{\mathbf{n}}\} \tag{25}$$

The matrix $[\mathbf{B}^{\mathbf{u}}]$ was defined in Equation (18) and $[\mathbf{B}^{\boldsymbol{\psi}}]$ is given as

$$[\mathbf{B}^{\boldsymbol{\psi}}] = \begin{bmatrix} 0 & \partial_z & -\partial_y \\ -\partial_z & 0 & \partial_x \\ \partial_y & -\partial_x & 0 \end{bmatrix} [\mathbf{N}^{\boldsymbol{\psi}}] \tag{26}$$

Equation (12) then yields the finite-element equations

$$[\mathbf{m}]\{\ddot{\mathbf{u}}^{\mathbf{n}}\} + [\mathbf{K}^{\mathbf{uu}}]\{\mathbf{u}^{\mathbf{n}}\} + [\mathbf{K}^{\mathbf{u}\boldsymbol{\psi}}]\{\boldsymbol{\psi}^{\mathbf{n}}\} = \int_V [\mathbf{B}^{\mathbf{u}}]^{\mathrm{T}}\{\boldsymbol{\sigma}^{\mathbf{r}}\}\,\mathrm{d}V + \int_V [\mathbf{N}^{\mathbf{u}}]^{\mathrm{T}}\{\mathbf{b}\}\,\mathrm{d}V + \int_S [\mathbf{N}^{\mathbf{u}}]^{\mathrm{T}}\{\mathbf{t}\}\,\mathrm{d}S$$
$$[\mathbf{K}^{\boldsymbol{\psi}\mathbf{u}}]\{\mathbf{u}^{\mathbf{n}}\} + [\mathbf{K}^{\boldsymbol{\psi}\boldsymbol{\psi}}]\{\boldsymbol{\psi}^{\mathbf{n}}\} = \int_V [\mathbf{B}^{\boldsymbol{\psi}}]^{\mathrm{T}}\{\mathbf{E}^{\mathbf{r}}\}\,\mathrm{d}V - \int_S [\mathbf{B}^{\boldsymbol{\psi}}]^{\mathrm{T}}\phi\{\mathbf{n}\}\,\mathrm{d}S \tag{27}$$

where

$$[\mathbf{K}^{\mathbf{uu}}] = \int_V [\mathbf{B}^{\mathbf{u}}]^{\mathrm{T}}[\mathbf{c}^{\mathbf{D}}][\mathbf{B}^{\mathbf{u}}]\,\mathrm{d}V, \quad [\mathbf{K}^{\mathbf{u}\psi}] = -\int_V [\mathbf{B}^{\mathbf{u}}]^{\mathrm{T}}[\mathbf{h}][\mathbf{B}^{\psi}]\,\mathrm{d}V$$
$$[\mathbf{K}^{\psi\mathbf{u}}] = -\int_V [\mathbf{B}^{\psi}]^{\mathrm{T}}[\mathbf{h}]^{\mathrm{T}}[\mathbf{B}^{\mathbf{u}}]\,\mathrm{d}V, \quad [\mathbf{K}^{\psi\psi}] = \int_V [\mathbf{B}^{\psi}]^{\mathrm{T}}[\boldsymbol{\beta}^{\varepsilon}][\mathbf{B}^{\psi}]\,\mathrm{d}V \tag{28}$$
$$[\mathbf{m}] = \int_V [\mathbf{N}^{\mathbf{u}}]^{\mathrm{T}}\rho[\mathbf{N}^{\mathbf{u}}]\,\mathrm{d}V$$

and

$$\{\boldsymbol{\sigma}^{\mathbf{r}}\} = [\mathbf{c}^{\mathbf{D}}]\{\boldsymbol{\varepsilon}^{\mathbf{r}}\} - [\mathbf{h}]\{\mathbf{P}^{\mathbf{r}}\}$$
$$\{\mathbf{E}^{\mathbf{r}}\} = -[\mathbf{h}]^{\mathrm{T}}\{\boldsymbol{\varepsilon}^{\mathbf{r}}\} + [\boldsymbol{\beta}^{\varepsilon}]\{\mathbf{P}^{\mathbf{r}}\} \tag{29}$$

Note that $\{\mathbf{n}\}$ represents the unit vector normal to the surface S. Also note that $[\mathbf{K}^{\mathbf{uu}}]$ and $\{\boldsymbol{\sigma}^{\mathbf{r}}\}$ defined in Equations (28) and (29) are different from those defined in Equations (20) and (21). Any possible confusion can be avoided by noting the other matrices and vectors that $[\mathbf{K}^{\mathbf{uu}}]$ and $\{\boldsymbol{\sigma}^{\mathbf{r}}\}$ are grouped with.

3.3. Stiffness matrix characteristics

For the solution of Equations (19) or (28) it is useful to know if the stiffness matrix is symmetric and if it is positive definite or non-definite. First note that the total stiffness matrices,

$$\begin{bmatrix} [\mathbf{K}^{\mathbf{uu}}] & [\mathbf{K}^{\mathbf{u}\phi}] \\ [\mathbf{K}^{\phi\mathbf{u}}] & [\mathbf{K}^{\phi\phi}] \end{bmatrix}$$

from the standard formulation and

$$\begin{bmatrix} [\mathbf{K}^{\mathbf{uu}}] & [\mathbf{K}^{\mathbf{u}\psi}] \\ [\mathbf{K}^{\psi\mathbf{u}}] & [\mathbf{K}^{\psi\psi}] \end{bmatrix}$$

from the vector potential formulation, are both symmetric. Note that the symmetry of the stiffness matrix for the scalar potential formulation is dependent upon the minus sign appearing in front of the $D_i\delta E_i$ term in the weak form of Equation (11).

Now let us define a stable piezoelectric material as one in which the material stiffness matrix

$$\begin{bmatrix} [\mathbf{c}^{\mathbf{D}}] & -[\mathbf{h}] \\ -[\mathbf{h}]^{\mathrm{T}} & [\boldsymbol{\beta}^{\varepsilon}] \end{bmatrix}$$

is positive definite. A material with positive definite stiffness requires a positive amount of work to be done on it in order to change the strain or electric displacement from the stress and electric field free state. In other words, the stored internal energy density of the material

$$U = \tfrac{1}{2}(\{\boldsymbol{\varepsilon}\}^{\mathrm{T}} - \{\boldsymbol{\varepsilon}^{\mathbf{r}}\}^{\mathrm{T}})[\mathbf{c}^{\mathbf{D}}](\{\boldsymbol{\varepsilon}\} - \{\boldsymbol{\varepsilon}^{\mathbf{r}}\}) - (\{\boldsymbol{\varepsilon}\}^{\mathrm{T}} - \{\boldsymbol{\varepsilon}^{\mathbf{r}}\}^{\mathrm{T}})[\mathbf{h}](\{\mathbf{D}\} - \{\mathbf{P}^{\mathbf{r}}\})$$
$$+ \tfrac{1}{2}(\{\mathbf{D}\}^{\mathrm{T}} - \{\mathbf{P}^{\mathbf{r}}\}^{\mathrm{T}})[\boldsymbol{\beta}^{\varepsilon}](\{\mathbf{D}\} - \{\mathbf{P}^{\mathbf{r}}\}) \tag{30}$$

is greater than zero for any strain and electric displacement combination not equal to the remanent state. Hence, when the material stiffness is positive definite, it can be readily shown that the stiffness matrix for the vector potential formulation

$$\begin{bmatrix} [\mathbf{K}^{uu}] & [\mathbf{K}^{u\psi}] \\ [\mathbf{K}^{\psi u}] & [\mathbf{K}^{\psi\psi}] \end{bmatrix}$$

is also positive definite. However,

$$\begin{bmatrix} [\mathbf{K}^{uu}] & [\mathbf{K}^{u\phi}] \\ [\mathbf{K}^{\phi u}] & [\mathbf{K}^{\phi\phi}] \end{bmatrix},$$

the stiffness matrix for the scalar potential formulation, is non-definite. Therefore, solutions to boundary value problems using the vector potential formulation exist at a global minimum in nodal degree of freedom space, while solutions for the scalar potential formulation lie on a saddle point. Furthermore, the positive definiteness of the stiffness matrix for the vector potential formulation lends itself to efficient iterative solution techniques like the conjugate gradient method [4].

3.4. System size

It is of interest to note that for the full three-dimensional case, the standard scalar potential formulation requires four degrees of freedom per node, three displacements and the electric potential. Unfortunately, the vector potential formulation requires six degrees of freedom per node, three displacements and three components of the vector potential. Hence, an increase in the size of the matrix system to be solved, by twice the number of nodes, is required for three-dimensional problems with the vector potential formulation.

Fortunately, the increase in system size from the scalar to the vector potential formulations in three dimensions does not exist in two dimensions. The nodal degrees of freedom required for in-plane, two-dimensional problems with the scalar and vector potential formulations are $\{u_x\ u_y\ \phi\}$ and $\{u_x\ u_y\ \psi_z\}$, respectively. Hence, the system sizes for two-dimensional problems are the same for both formulations.

4. COMPARISON OF THE METHODS FOR A COUPLED LINEAR PIEZOELECTRIC PROBLEM

In this section, numerical tests are presented to illustrate and compare the convergence rates of the scalar and vector potential formulations with respect to mesh size. The two numerical methods will be compared to an exact, two-dimensional solution of Equations (1)–(10) with no body forces, no volume charge density, zero remanent state and no inertia, i.e. $b_i = 0$, $q^v = 0$, $\varepsilon_{ij}^{\mathrm{r}} = 0$, $P_i^{\mathrm{r}} = 0$ and $\rho = 0$. A solution for the scalar potential, vector potential and displacements is,

$$\phi = \phi_0 \sinh \alpha x \cos \pi y \tag{31}$$

$$\psi_z = \psi_0 \cosh \alpha x \sin \pi y \tag{32}$$

$$u_x = u_0 \sinh \alpha x \cos \pi y \tag{33}$$

$$u_y = v_0 \cosh \alpha x \sin \pi y \tag{34}$$

where

$$\alpha = 3.9432\,\mathrm{m}^{-1}, \quad \psi_0 = 1.0551 \times 10^{-8}\,\mathrm{C/Vm}\ \phi_0$$

$$u_0 = 5.1001 \times 10^{-10}\,\mathrm{m/V}\ \phi_0, \quad v_0 = -1.2175 \times 10^{-9}\,\mathrm{m/V}\ \phi_0$$

and ϕ_0 is an arbitrary electrical loading variable with dimensions of voltage. For this study ϕ_0 is taken to be equal to one. This solution is valid for a material with piezoelectric properties characteristic of PZT aligned in the x-direction, such that the simplified two-dimensional constitutive behaviour of the material can be written as

$$\varepsilon_{xx} = s_{33}\sigma_{xx} + s_{31}\sigma_{yy} + d_{33}E_x \tag{35}$$

$$\varepsilon_{yy} = s_{31}\sigma_{xx} + s_{33}\sigma_{yy} + d_{31}E_x \tag{36}$$

$$2\varepsilon_{xy} = 2(s_{33} - s_{31})\sigma_{xy} + d_{15}E_y \tag{37}$$

$$D_x = d_{33}\sigma_{xx} + d_{31}\sigma_{yy} + \kappa E_x \tag{38}$$

$$D_y = d_{15}\sigma_{xy} + \kappa E_y \tag{39}$$

$$s_{33} = 1.6667 \times 10^{-11}\,\mathrm{N/m^2}, \quad s_{31} = -6.1667 \times 10^{-12}\,\mathrm{N/m^2}, \quad \kappa = 2.0011 \times 10^{-8}\,\mathrm{C/Vm}$$

$$d_{33} = 4.5 \times 10^{-10}\,\mathrm{m/V}, \quad d_{31} = -2.1 \times 10^{-10}\,\mathrm{m/V} \quad d_{15} = 5.8 \times 10^{-10}\,\mathrm{m/V}$$

Note that the stresses, strains, tractions, electric fields, electric displacements and surface charge densities can be readily determined from the solution given in Equations (31)–(34).

Two sets of boundary value problems have been solved with the finite-element methods described in Section 3. The region considered is a square, 8 m long on each side, as illustrated in Figure 1. The region is divided into square, fully integrated, 9-noded Lagrange elements. The length of a side of one element is given as h. The two sets of boundary value problems solved will be called the Dirichlet BC problems and the Neumann BC problems. For the scalar potential formulation, the scalar electric potential and the displacements given by Equations (31), (33) and (34) are specified at the nodes on the external boundary for the Dirichlet BC problem. For the Neumann BC problem, the tractions and surface charge density are specified on the outer boundary. For the vector potential formulation, the vector potential and the displacements given by Equations (32)–(34) are specified at the nodes for the Dirichlet BC problem. Finally, for the vector potential formulation Neumann BC problem, the tractions and the electric potential ϕ associated with the solution given by Equations (31)–(34) are specified on the outer boundary.

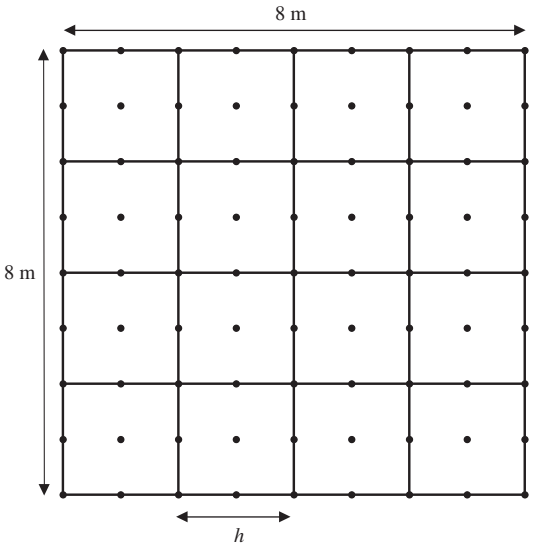

Figure 1. The finite-element mesh used for the study of convergence with respect to mesh size.

In order to determine the convergence characteristics of each method with respect to mesh refinement, the following energy norm is considered.

$$e = \frac{\int_V \sigma_{ij}^{\mathrm{err}} \varepsilon_{ij}^{\mathrm{err}} + E_i^{\mathrm{err}} D_i^{\mathrm{err}} \, \mathrm{d}V}{\int_V \sigma_{ij}^{\mathrm{ex}} \varepsilon_{ij}^{\mathrm{ex}} + E_i^{\mathrm{ex}} D_i^{\mathrm{ex}} \, \mathrm{d}V} \tag{40}$$

The numerator in Equation (40) represents twice the stored energy associated with the error in the numerical solution, and the denominator is twice the stored energy in the solid computed from the exact solution (superscript ex). The quantities $\sigma_{ij}^{\mathrm{err}}$, $\varepsilon_{ij}^{\mathrm{err}}$, E_i^{err} and D_i^{err} are computed from the errors in the finite-element quantities (superscript FE), e.g. for the scalar potential formulation $\phi^{\mathrm{err}} = \phi^{\mathrm{ex}} - \phi^{\mathrm{FE}}$ and $u_i^{\mathrm{err}} = u_i^{\mathrm{ex}} - u_i^{\mathrm{FE}}$, then $E_i^{\mathrm{err}} = -\phi_{,i}^{\mathrm{err}}$, $\varepsilon_{ij}^{\mathrm{err}} = (u_{i,j}^{\mathrm{err}} + u_{j,i}^{\mathrm{err}})/2$, $\sigma_{ij}^{\mathrm{err}} = c_{ijkl}^{E} \, \varepsilon_{kl}^{\mathrm{err}} - e_{kij} E_k^{\mathrm{err}}$, and $D_i^{\mathrm{err}} = e_{ikl} \varepsilon_{kl}^{\mathrm{err}} + \kappa_{ij}^{\varepsilon} E_j^{\mathrm{err}}$. These quantities are evaluated at the integration stations of the elements and the appropriate products are integrated over the volume of the region.

Figure 2 plots the energy norm, e, as a function of the mesh size, h, on a logarithmic scale for each type of problem. Note that e must go to zero as h goes to zero if the method is convergent. On this plot, h ranges from 0.25 to 8 corresponding to 1024 elements and one element in the mesh, respectively. Note the following observations from Figure 2. First, the wavelength of the loading for this problem corresponds to a mesh size of $h = 2$. Therefore, mesh sizes greater than 2 cannot be expected to yield accurate results. Furthermore, as seen on Figure 2, the energy norm is erratic for $h > 2$. For mesh sizes less than 2, both the scalar and vector potential formulations appear to have essentially identical rates of convergence with respect to mesh size. For both formulations, the magnitude of the energy norm is smaller for the Dirichlet BC problems than for the Neumann BC problems by approximately a factor of 2.

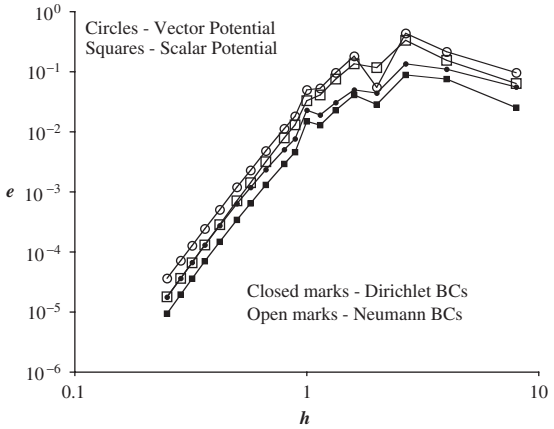

Figure 2. Plots of the energy norm, e, defined in Equation (40) as a function of the mesh size, h.

Finally, for both types of boundary conditions, the magnitude of the energy norm is smaller for the scalar potential formulation than the vector potential formulation by approximately a factor of 2.

5. NUMERICAL STABILITY FOR NON-LINEAR ELECTRICAL PROBLEMS

To this point it has been assumed that the remanent strain and polarization states remain fixed, and the problem is linear. However, the primary reason for introducing the vector potential formulation is due to its stability for solving non-linear problems. Specifically, the vector potential formulation is most useful when the electric field versus electric displacement relationship is characteristic of ferroelectric ceramics. To investigate the effectiveness of the scalar and vector potential formulations for solving non-linear electrical problems, the stability of a simple, fixed-point, iterative solution scheme for a single-degree-of-freedom electrical system will be determined. The non-linear constitutive law used for this problem is highly simplified, but it does contain the essential feature of ferroelectric behaviour required to understand the stability of the two numerical methods.

Consider the non-linear electrical constitutive relationship given by

$$\begin{aligned} D &= \kappa E, \quad P^{\mathrm{r}} = 0 \quad \text{if } E \leqslant E_0 \\ D &= \kappa E + P^{\mathrm{r}}, \quad P^{\mathrm{r}} = (H - \kappa)(E - E_0) \quad \text{if } E \geqslant E_0 \end{aligned} \tag{41}$$

where E_0 is the coercive field, and the hardening modulus, H, is greater than the initial dielectric permittivity κ for ferroelectric materials. For the scalar potential formulation, the single-degree-of-freedom system considered is a one-dimensional capacitor with the electric displacement fixed across it. The proposed iterative solution procedure is given by

$$E^{i+1} = \frac{1}{\kappa}(D - P^{\mathrm{r},i}) \tag{42}$$

where D is the fixed electric displacement, E^{i+1} is the electric field computed at the $i+1$th iteration, and $P^{r,i}$ is the remanent polarization computed from Equation (41) after the ith solution step. Then, for levels of electric field greater than the coercive field, Equation (41) can be used in (42) to yield

$$E^{i+1} = \left(1 - \frac{H}{\kappa}\right) E^i + \frac{1}{\kappa} D - \left(1 - \frac{H}{\kappa}\right) E_0 \tag{43}$$

From Equation (43) it can be readily seen that this iterative method is unstable if $H/\kappa > 2$, and the solution for E oscillates if $H/\kappa > 1$. For most ferroelectric materials of technological interest $H/\kappa > 2$, and this solution method will be unstable.

The analogous single-degree-of-freedom system for the vector potential formulation has the applied electric field fixed across the one-dimensional capacitor. The iterative scheme analogous to Equation (42) is

$$D^{i+1} = \kappa E + P^{r,i} \tag{44}$$

implying that

$$D^{i+1} = \kappa E_0 + H(E - E_0) \tag{45}$$

Notice that Equation (45) will converge to the exact solution after two iterations, i.e. the first iteration will predict that $D^1 = \kappa E$ and then the second will reach the exact solution given by Equation (45).

It is true that a more sophisticated iterative solution scheme, such as a Newton–Raphson method, could provide a solution for the scalar potential formulation. However, for certain problems involving the integration of constitutive response along streamlines, the procedure represented by Equation (43) is the only one available. For example, many authors have relied on this procedure to solve for the fields around a steadily growing crack in a material with a path dependent constitutive behaviour, see for example Reference [5]. Furthermore, this simple iterative solution procedure requires only one inversion of the system stiffness matrix, while Newton–Raphson methods require an inversion at each step. Hence, for some problems this solution method is the only scheme available, and for some problems this method can provide savings in computational time.

6. COMPARISON OF A CALCULATED CRACK TIP FIELD TO AN ANALYTICAL SOLUTION

In this section, the vector potential formulation is implemented to solve an uncoupled, non-linear electrical problem and compared with a known analytical solution. The physical problem is to determine the distributions of electric field and electric displacement very close to a crack tip in an electrically non-linear material with an electrically conducting medium in the space between the crack faces. All mechanical coupling is ignored and the specific form of the electrical constitutive law is given in Equation (48). From a fracture mechanics perspective, this problem is analogous to analysing the plastic zone around a crack tip under small scale yielding conditions. A simple semi-circular radial mesh is used for this problem. The mesh contains 1926 nodes and 625 8-noded isoparametric elements with four integration stations each. Every node has one degree of freedom, ψ_z, associated with it. The mesh and

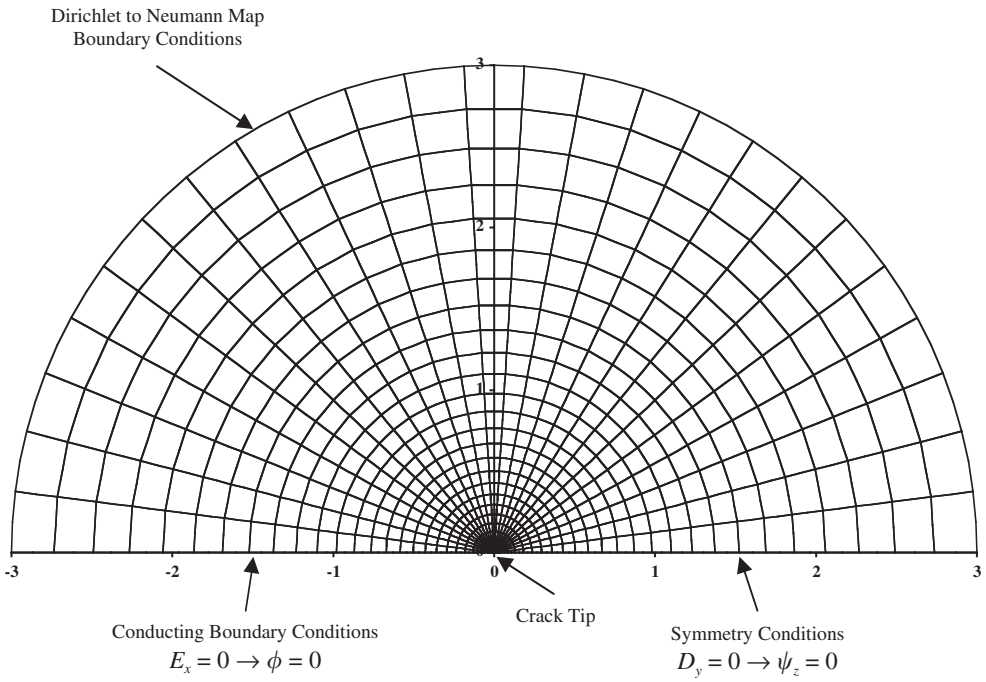

Figure 3. The finite-element mesh used for the solution of the electrical fields around a crack tip. The mesh consists of 1926 nodes and 625 8-noded isoparametric elements. Conducting boundary conditions are applied to the crack surface and symmetry conditions are applied ahead of the crack tip. A so-called Dirichlet to Neumann map is applied to the outer circular boundary to account for material outside of the mesh and the far field loading conditions. The co-ordinate axes are normalized by the size of the non-linear switching region R_s.

the boundary conditions are shown in Figure 3. The co-ordinate axes are normalized by the size of the non-linear switching zone, R_s. Note that a Dirichlet to Neumann map [6, 7] is applied to the outer circular boundary in order to simulate the appropriate asymptotic crack tip conditions and the response of the material outside of the mesh. The far field solution and the size of the switching zone are given by

$$\psi_z \rightarrow \kappa K_E \sqrt{\frac{2}{\pi}} \operatorname{Im}[(x + \mathrm{i}y)^{1/2}] \quad \text{as } |x + \mathrm{i}y| \rightarrow \infty \tag{46}$$

and

$$R_s = \frac{1}{2\pi} \left(\frac{K_E}{E_0} \right)^2 \tag{47}$$

where κ is the linear dielectric permittivity, K_E is an electric field intensity factor, and E_0 is the coercive field.

A simple constitutive law is assumed where the electric displacement is always aligned with the electric field. The relationship between the magnitude of the electric field, E, and

the magnitude of the electric displacement, D, is specified by

$$E = \begin{cases} D/\kappa & \text{if } D < D_0 \\ E_0 & \text{if } D_0 \leqslant D \leqslant D_L \\ E_0 + (D - D_L)/\kappa & \text{if } D > D_L \end{cases} \tag{48}$$

where $D_0 = \kappa E_0$. This constitutive law is shown schematically on the inset in Figure 4. The variational form of the procedure used to solve this non-linear problem, analogous to Equation (27), is given by

$$\int_V \frac{1}{\kappa} D_i \delta D_i \, \mathrm{d}V = \int_V \frac{1}{\kappa} P_i^{\mathrm{r}} \delta D_i \, \mathrm{d}V - \int_S \phi n_i \delta D_i \, \mathrm{d}S \tag{49}$$

The left-hand side yields the stiffness matrix dotted with the vector of unknown nodal degrees of freedom. The second term on the right-hand side produces a nodal driving potential vector along with contributions to the stiffness arising from the Dirichlet to Neumann map. Finally, the first term on the right-hand side accounts for the material non-linearity, with the remanent polarization evaluated from the solution to the previous iteration. Note that the remanent polarization is in the direction of the applied electric field, and its magnitude can be derived from Equation (48) as

$$P^{\mathrm{r}} = \begin{cases} 0 & \text{if } D < D_0 \\ D - D_0 & \text{if } D_0 \leqslant D \leqslant D_L \\ D_L - D_0 & \text{if } D > D_L \end{cases} \tag{50}$$

The analytical solution for this problem and the associated details are reported in Reference [8]. Outside of the switching region the solution is given as

$$E_y + \mathrm{i}E_x = \frac{\mathrm{i}K_E}{[2\pi(x - X_{\mathrm{s}} + \mathrm{i}y)]^{1/2}} \quad \text{for } |x - X_{\mathrm{s}} + \mathrm{i}y| \geqslant R_{\mathrm{s}} \tag{51}$$

where the centre of the zone of non-linear behaviour is located on the x-axis at

$$X_{\mathrm{s}} = R_{\mathrm{s}} \left[1 - 2 \frac{D_L/D_0 - 1 + \ln(D_0/D_L)}{(D_L/D_0 - 1)^2} \right] \tag{52}$$

Within the switching zone the solution is given by

$$\begin{aligned} E_{\bar{r}} &= E_0, \quad E_{\bar{\theta}} = D_{\bar{\theta}} = 0, \quad D_{\bar{r}} = \frac{2R_{\mathrm{s}} D_0}{\bar{r}} \cos\bar{\theta} \quad \text{for } 2R_L \cos\bar{\theta} \leqslant \bar{r} \leqslant 2R_{\mathrm{s}} \cos\bar{\theta} \\ \bar{r} &= \sqrt{(x - X_{\mathrm{s}} + R_{\mathrm{s}})^2 + y^2}, \quad \bar{\theta} = \arctan \frac{y}{x - X_{\mathrm{s}} + R_{\mathrm{s}}} \end{aligned} \tag{53}$$

where the $(\bar{r}, \bar{\theta})$ co-ordinate system originates behind the crack tip where the switching zone intersects the x-axis, and the radius of the lock-up region is given as

$$R_L = \frac{D_0}{D_L} R_{\mathrm{s}} \tag{54}$$

The solution within the lock-up zone cannot be written in simple closed form with electric fields as functions of co-ordinates as in Equations (51)–(53). Instead the solution is given for the co-ordinates as a function of the electric field components. Contours of constant electric

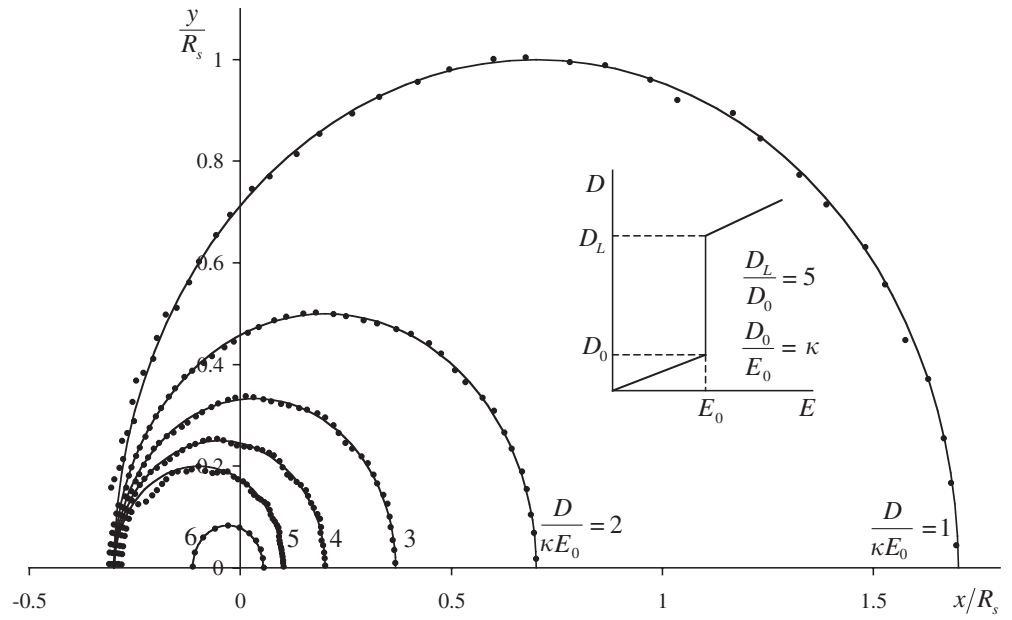

Figure 4. Contours of constant electric displacement magnitude near the crack tip. The dots represent the numerical finite-element results and the curves are the analytical solution from Reference [8]. The inset is a schematic of the non-linear material constitutive law used for the calculation. Notice that very large gradients of electric displacement occur at the left edge of the switching zone. Also note that only every fifth numerical point was plotted on the contour for $D/\kappa E_0 = 6$ in order to reveal the agreement with the analytical result.

field magnitude, E, are circles of radius $R(E)$ centred on the x-axis at position $X(E)$. The formulas for $R(E)$ and $X(E)$ are

$$R(E) = R_s \frac{1}{E/E_0(E/E_0 + D_L/D_0 - 1} \quad \text{for } E \geqslant E_0 \tag{55}$$

$$X(E) = 2R_s \left[\frac{1 - D_L/D_0 + (E/E_0 + D_L/D_0 - 1)\ \ln((E/E_0 + D_L/D_0 - 1)/E/E_0)}{(E/E_0 + D_L/D_0 - 1)(D_L/D_0 - 1)^2} \right] - R(E) \quad \text{for } E \geqslant E_0 \tag{56}$$

A description of how the field direction is determined is given in Reference [8], but for the sake of brevity it will not be given here. Equations (55) and (56) will suffice for the comparison to the numerical results given in Figure 4. The associated contours of constant electric displacement can then be determined with the aid of the constitutive law given by Equation (48).

For the example shown in Figure 4 the ratio of D_L/D_0 was taken to be equal to 5. The iterative procedure was allowed to proceed for 2864 steps, with the entire calculation taking approximately 7 minutes on a Silicon Graphics O2000 workstation. Figure 4 plots contours of constant electric displacement magnitude from the results of the numerical calculation

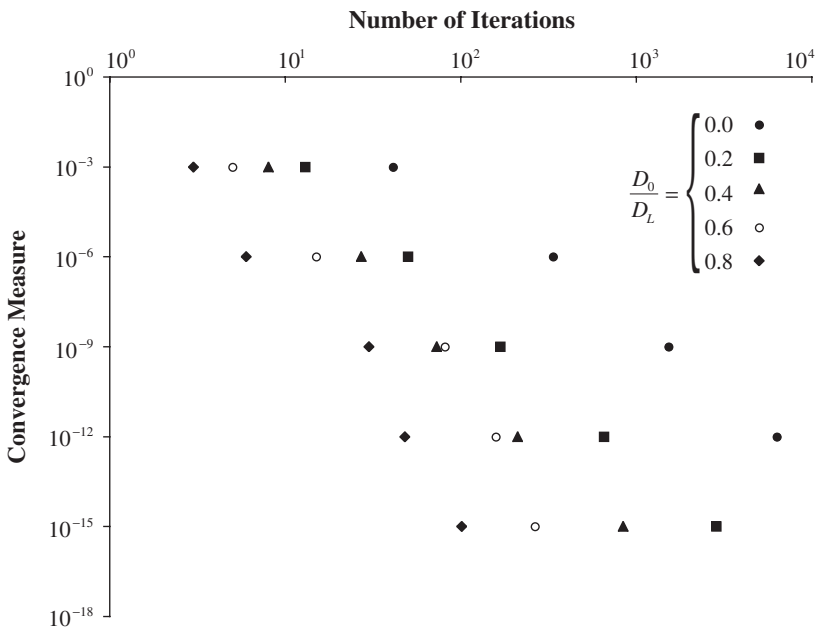

Figure 5. Plots of a measure of convergence (the sum over all nodes of the square of the difference of the nodal quantity between iterations) versus the number of iterations required to reach that level of convergence as a function of the constitutive parameter D_0/D_L.

(dots interpolated from the nearest integration stations) against the analytical solution (lines) described by Equations (51)–(56). To monitor the convergence of the solution scheme, the sum over all nodes of the square of the difference between ψ_z at the current step and ψ_z at the previous iteration was computed. This quantity obtained values of 10^{-3}, 10^{-6}, 10^{-9}, 10^{-12}, and 10^{-15} after 13, 50, 168, 654 and 2864 iterations, respectively. Note that a similar solution procedure was attempted for this problem with a scalar potential formulation; however, convergence was not achieved as predicted by the analysis of Section 5.

For this problem the rate of convergence with respect to the number of numerical iterations depends on the ratio D_0/D_L, which can range from 0 to 1. Of course for $D_0/D_L = 1$, the problem is entirely linear and the method converges after only one iteration. Figure 5 plots the previously described measure of convergence versus the number of iterations required to reach that level of convergence. The measure of convergence is simply the sum over all nodes of the square of the difference between ψ_z at the current step and ψ_z at the previous iteration. Note that in general, as D_0/D_L decreases the number of iterations required to attain a given level convergence increases. Furthermore, recall that Figure 4 illustrates the accuracy of the solution when the convergence measure reaches the level of 10^{-15}.

7. CONCLUDING REMARKS

A new finite-element formulation for the solution of electromechanical boundary value problems based on an electrical vector potential has been developed. The method requires two

extra degrees of freedom per node over the standard formulation for three-dimensional problems, and it cannot be used for problems where a volumetric free charge density must be considered. However, the method yields a positive definite stiffness matrix for stable electromechanical materials, and it exhibits superior numerical stability over the standard formulation for problems with electrically non-linear material behaviour characteristic of ferroelectric ceramics. Furthermore, for two-dimensional problems, the vector potential formulation yields the same number of degrees of freedom per node as the scalar potential formulation.

The formulations presented in Section 3 are sufficiently general. Specific forms for the interpolation functions in Equations (16) and (24) and for the non-linear description of the remanent state of the material were not given. Appropriate forms of the interpolation functions required to ensure spatial convergence of the solution can be found in many texts, e.g. Reference [9], and forms for the constitutive law describing the evolution of the remanent state are given in Reference [10]. Lastly, the new vector potential formulation provides a numerical tool for the investigation of electromechanical fields in structures like the piezoelectric stack actuator, and around structural features like electrodes and crack tips.

REFERENCES

1. Allik H, Hughes TJR. Finite element method for piezoelectric vibration. *International Journal for Numerical Methods in Engineering* 1970; **2**:151–157.
2. Benjeddou A. Advances in piezoelectric finite-element modeling of adaptive structural elements: a survey. *Computers and Structures* 2000; **76**:347–363.
3. Ghandi K, Hagood NW. A hybrid finite-element model for phase transition in nonlinear electro-mechanically coupled material. In *Smart Structures and Materials 1997: Mathematics and Control in Smart Structures*, Proceedings of SPIE Volume 3039. Varadan VV, Chandra J, (eds). Washington: SPIE, 1997; 97–112.
4. Axelsson O. *Iterative Solution Methods*. Cambridge University Press, Cambridge 1994.
5. Dean RH, Hutchinson JW. Quasi-static steady crack growth in small-scale yielding. In *American Society for Testing and Materials*. Fracture Mechanics: 12th Conference, ASTM STP 700, 1980; 383–405.
6. Givoli D, Keller JB. A finite-element method for large domains. *Computer Methods in Applied Mechanics and Engineering* 1989; **76**:41–66.
7. Givoli D, Rivkin L. The DtN finite-element method for elastic domains with cracks and re-entrant corners. *Computers and Structures* 1993; **49**:633–642.
8. Landis CM. Uncoupled, asymptotic mode III and mode E crack tip solutions in non-linear ferroelectric materials. *Engineering Fracture Mechanics* 2002; **69**:13–23.
9. Bathe KJ. *Finite Element Procedures*. Prentice-Hall: New Jersey, 1996.
10. Landis CM. Fully coupled, multi-axial, symmetric constitutive laws for polycrystalline ferroelectric ceramics. *Journal of the Mechanics and Physics of Solids* 2002; **50**:127–152.

